

Probing The Multiphase Interstellar Medium Of The Dwarf Starburst Galaxy NGC 625 With *FUSE* Spectroscopy¹

John M. Cannon

Max-Planck-Institut für Astronomie, Königstuhl 17, D-69117, Heidelberg, Germany

cannon@mpia.de

Evan D. Skillman

Department of Astronomy, University of Minnesota, 116 Church St. S.E., Minneapolis, MN 55455

skillman@astro.umn.edu

Kenneth R. Sembach

Space Telescope Science Institute, 3700 San Martin Drive, Baltimore, MD 21218

sembach@stsci.edu

Dominik J. Bomans

Astronomisches Institut, Ruhr-Universität Bochum, Universitätsstr. 150, 44780, Bochum, Germany

bomans@astro.ruhr-uni-bochum.de

ABSTRACT

We present new *FUSE* spectroscopy of the dwarf starburst galaxy NGC 625. These observations probe multiple phases of the interstellar medium, including the coronal, ionized, neutral and molecular gas. This nearby ($D = 3.9 \pm 0.2$ Mpc) system shows a clear detection of outflowing coronal gas as traced by O VI $\lambda 1032$ Å absorption. The centroid of the O VI profile is blueshifted with respect to the galaxy systemic velocity by ~ 30 km s⁻¹, suggesting a low-velocity outflow. The implied O VI velocity extent is found to be 100 ± 20 km s⁻¹, which is fully consistent with the detected H I outflow velocity found in radio synthesis

observations. We detect multiple lines of diffuse H₂ absorption from the ISM of NGC 625; this is one of only a few extragalactic systems with *FUSE* detections of H₂ lines in the Lyman and Werner bands. We find a potential abundance offset between the neutral and nebular gas that exceeds the errors on the derived column densities. Since such an offset has been found in multiple dwarf galaxies, we discuss the implications of a lower-metallicity halo surrounding the central star forming regions of dwarf galaxies. The apparent offset may be due to saturation of the observed O I line, and higher S/N observations are required to resolve this issue.

Subject headings: galaxies: starburst — galaxies: dwarf — galaxies: abundances — galaxies: kinematics and dynamics — galaxies: individual (NGC 625)

1. Introduction

Local starbursting dwarf galaxies offer a unique opportunity to study the various phases of the interstellar medium (ISM) under extreme conditions and in unprecedented detail. Furthermore, the physical conditions in these targets are likely very similar to those found in galaxies at high redshifts, making them crucial benchmarks against which observations of such targets must be compared. With these observations, we capitalize on the high-resolution capabilities of the *Far Ultraviolet Spectroscopic Explorer* (*FUSE*; see Moos et al. 2000) to observe the interaction of the multiple phases of the ISM in NGC 625, a nearby ($D = 3.9 \pm 0.2$ Mpc; Cannon et al. 2003), low mass ($M_{\text{HI}} = 1.1 \times 10^8 M_{\odot}$; Cannon et al. 2004), low metallicity ($12 + \log(\text{O}/\text{H}) = 8.14 \pm 0.02$; Skillman et al. 2003b) dwarf irregular galaxy in the Sculptor Group that is currently undergoing a massive star formation episode (see Table 1 for basic galaxy properties).

Of paramount importance in the evolution of dwarf galaxies is the role played by outflows powered by the energy inputs of supernovae and stellar winds. These outflows may drive significant fractions of the gas from galaxies with shallow potential wells. Recent simulations suggest that the return of metals into the intergalactic medium (IGM) finds its most effective avenue in these low mass galaxies (Mac Low & Ferrara 1999). Understanding the nature of these outflows is therefore a fundamental astrophysical problem with far-reaching implications. These *FUSE* spectra isolate the powerful diagnostic absorption lines of O VI

¹Based on observations made with the NASA-CNES-CSA *Far Ultraviolet Spectroscopic Explorer*. *FUSE* is operated for NASA by the Johns Hopkins University under NASA contract NAS 5-32985.

$\lambda\lambda 1032, 1038 \text{ \AA}$ which probe the temperature and kinematic structure of the coronal gas in a galaxy (see, e.g., Heckman et al. 2001). The O VI ion traces hot ionized gas over the temperature range $T \sim 10^5 - 10^6 \text{ K}$, with maximum sensitivity to gas in collisional ionization equilibrium at temperatures $T \sim (2 - 3) \times 10^5 \text{ K}$ (Sutherland & Dopita 1993). Thus, knowing the temperature of the emitting material, we can (with some assumptions) directly estimate electron density and pressure in the coronal gas. We can then assess the importance and timescale of radiative cooling in outflows and in the starburst phenomenon. Indeed, in a case such as NGC 625 where the outflow is of comparatively low velocity (see, e.g., Heckman et al. 2001), such effects may be dominant. These observations thus provide an opportunity to investigate many properties of outflows in dwarf galaxies.

Multiple independent lines of evidence suggest that the recent star formation in NGC 625 has been violent and that the coronal gas content is substantial. An extended soft x-ray component was detected in *ROSAT* imaging (Bomans & Grant 1998) and has been verified in newly-obtained *Chandra* imaging (Cannon et al., in preparation). To attain hot gas at large distances from the central starburst requires the presence of an outflow in the recent past. This outflow is also seen in H I synthesis imaging (Cannon et al. 2004), making NGC 625 one of only a few dwarf galaxies with a detected neutral gas outflow. This outflow appears to be a result of the extended (both spatially and temporally) star formation event that the galaxy has undergone over the last $\gtrsim 50 \text{ Myr}$ (see Cannon et al. 2003 for details). This extended burst is unexpected, given the brevity of star formation implied by the presence of the $\lambda 4686 \text{ \AA}$ spectroscopic Wolf-Rayet (W-R) feature ($\lesssim 6 \text{ Myr}$; see Conti 1991; Schaerer et al. 1999; the spectrum is presented in Skillman et al. 2003b).

Theoretical and observational evidence suggests that star formation behavior should be a function of metallicity (see, e.g., Maloney & Black 1988; Taylor et al. 1998). NGC 625 has a metallicity significantly below the solar value, $[\text{O}/\text{H}] = -0.47 \pm 0.06$ (Skillman et al. 2003b), which provides an opportunity to study the interplay between powerful starburst activity and molecular gas content at a metallicity similar to that of the Small Magellanic Cloud. Single-dish CO spectra reveal a large CO cloud coincident with the main dust concentration (Côté, Braine, & Cannon, in preparation), but offset from the current massive star formation regions. This position also hosts a moderately-extincted, low-mass stellar cluster that produces a thermal radio continuum peak (Cannon & Skillman 2004).

In light of these arguments, we also analyze the diffuse H_2 content of this relatively low-metallicity galaxy. The Lyman-Werner bands of H_2 are expected to be very sensitive to relatively cool diffuse H_2 gas ($T \sim 100 - 1000 \text{ K}$) over a wide range of column densities ($N(\text{H}_2) \sim 10^{14} - 10^{22} \text{ cm}^{-2}$). In observations of galaxies or large star-formation regions, these lines probe the diffuse H_2 content along many sightlines to ultraviolet (UV)-luminous sources.

Evidence suggests that diffuse H₂ clouds are indeed prevalent at low metallicities; Tumlinson et al. (2002) detect diffuse H₂ along 92% of sightlines toward UV sources in the SMC, which has very nearly the same metallicity (Dufour 1984; Garnett 1999) as NGC 625. However, integrated *FUSE* spectra of metal-poor starbursts suggest that diffuse H₂ is more difficult to detect in distant targets (Vidal-Madjar et al. 2000; Heckman et al. 2001; Thuan et al. 2002; Aloisi et al. 2003; Lebouteiller et al. 2004; Lecavelier des Etangs et al. 2004; Hoopes et al. 2004; see further discussion in § 4.2). With these data we add NGC 625 to the small but growing sample of dwarf starburst systems with *FUSE* observations of diffuse H₂ gas; we detect multiple H₂ lines and discuss the implied properties of the molecular gas.

Finally, since the spectral region probed by *FUSE* is rich in neutral and ionized gas absorption lines, we also address the column densities and abundances of observable species in the ISM of NGC 625. This point is especially important since evidence is growing for a bimodal abundance distribution in the ISM of dwarf galaxies. The nebular regions (i.e., near the star formation regions and accessible to abundance studies via optical and near-infrared emission line spectroscopy) appear to have elevated abundances compared to the neutral interstellar gas through which *FUSE* sightlines usually pass. The sample of dwarf systems with such an analysis is small, but the offsets appear to be pronounced (> 0.5 dex in oxygen abundance). With these arguments in mind, we analyze the neutral gas abundances in NGC 625 and compare these to values obtained from nebular spectroscopy obtained by Skillman et al. (2003b).

Understanding the kinematics and behavior of the outflowing coronal gas, the molecular gas content, and the neutral-gas abundances are the major goals of this work. With these data, we can characterize the interaction of the outflowing gas with the neutral components as revealed in our H I imaging and from other ionization species within the *FUSE* spectrum. In addition, they allow us to estimate the metallicity of the neutral gas and compare these values with those found for emission line gas in the nebular regions. We discuss the evolution of dwarf starburst galaxies using these *FUSE* data and published information in the literature.

2. Observations and Data Reduction

FUSE spectroscopy of NGC 625 using the $4'' \times 20''$ medium resolution aperture (MDRS) was obtained on 2003, November 8-9, for program D040. No roll angle constraints were placed on the observation, since the aperture width is comparable to the size of the high-equivalent width H α emission (and hence the most UV-luminous sightlines). Our observations were obtained with an average slit angle 112° east of north; the approximate aperture placement is shown superposed on *Hubble Space Telescope* (*HST*) WFPC2 V-band and (continuum

subtracted) H α images in Figure 1. The total integration time on-source was 58.1 ksec, with $\sim 76\%$ of this occurring during orbital night, which decreases the contamination of the spectra by terrestrial N I and O I airglow lines. Data from both orbital day and night were used in spectral regions not affected by airglow lines; otherwise, only data obtained during orbital night were used in our analysis of the NGC 625 absorption features.

This observation produced 23 raw time-tagged exposures which were re-processed using a recent version of the *FUSE* calibration software (CALFUSE v2.4) available from Johns Hopkins University². This pipeline reduction removes mirror, grating, and spacecraft motions, and then corrects for astigmatism and Doppler motions. Wavelengths are assigned to each photon, and these events are screened for data quality (e.g., event bursts, spacecraft jitter, etc.). The data are then flux calibrated and the bad pixel maps are corrected for spacecraft motions. Finally, spectral extractions are performed for each detector segment for each channel using either the orbital night-only data or the orbital day and night data. Each individual exposure was processed by the pipeline and the resulting spectra were combined to produce the final spectrum for each channel and data segment. This results in a total of 16 extracted spectra.

FUSE uses four optical channels to produce 8 detector segments that allow spectral extractions between ~ 900 and 1200 \AA . The two SiC channels are optimized for shorter wavelengths (905 to 1100 \AA), while the LiF channels are optimized for longer wavelengths (980 to 1187 \AA). The LiF channels are more sensitive than the SiC channels, so these provide our highest signal-to-noise (S/N) data. The effective area of the telescope is also maximized at $\sim 1032 \text{ \AA}$ (i.e., very near the important O VI absorption features), so we concentrate our analysis on the LiF1 channel, with LiF2 (lower S/N) serving to verify detections. Data in the SiC channels are generally of low S/N (caused by a combination of lower effective area and channel misalignment between the LiF and SiC channels), and we do not use them in this analysis. We present in Figure 2 the LiF1A and LiF1B spectra of NGC 625, binned to 0.05 \AA resolution for clarity. Note the richness of the spectrum, with numerous strong absorption lines detected. We do not combine any of the overlapping detector segments, due to the changing spectral resolution and sensitivity of the detectors as a function of wavelength. The final velocity resolution is $\sim 30 \text{ km s}^{-1}$, with S/N ratios of ~ 10 and 5 per resolution element at 1032 \AA for the LiF1 and LiF2 channels, respectively. All velocities quoted are in the heliocentric reference frame.

²See <http://fuse.pha.jhu.edu/analysis/calfuse.html>

3. Analysis

These *FUSE* data probe four different ISM phases: diffuse molecular gas, neutral gas, warm photoionized gas, and hot coronal gas. We discuss the kinematics of each of these phases as derived from Gaussian fitting to the absorption profiles in the following subsection and summarize important line properties in Table 2. We then discuss derived column densities of the gas in § 3.2 and the inferred elemental abundances in § 3.3.

3.1. Gas Kinematics

There are two main absorbing components seen in these data. First, Milky Way gas appears near zero velocity. Second, NGC 625 absorptions are centered around $+400 \text{ km s}^{-1}$. In addition, there may also exist a halo intermediate-velocity cloud as seen in the red wings of some of the stronger Milky Way absorption lines (see below). In this work we concentrate on the lines arising within NGC 625.

Beginning with the molecular phase, we detect numerous low-level H_2 absorption lines in NGC 625. The Lyman and Werner bands of H_2 produce hundreds of absorption lines in the spectral region under study. The lowest rotational levels ($J = 0, 1, \text{ and } 2$) are expected to be most highly-populated by the moderate diffuse molecular hydrogen columns and temperatures typically found in external galaxies ($N(\text{H}_2) \sim 10^{14} - 10^{16} \text{ cm}^{-2}$; $T \sim 100 - 1000 \text{ K}$). Of these low-level lines, six are detected in unblended, high S/N regions of the final spectra. We do not detect any lines in the higher J levels. The velocity centroid of the detected lines (including R(0)(2-0) $\lambda 1077.1399 \text{ \AA}$, R(1)(4-0) $\lambda 1049.960 \text{ \AA}$, R(2)(5-0) $\lambda 1038.689 \text{ \AA}$, P(1)(5-0) 1038.157 \AA , R(2)(0-0) $\lambda 1009.024 \text{ \AA}$, and R(1)(8-0) $\lambda 1002.449 \text{ \AA}$) is found to be $v_{\text{H}_2} = 401 \pm 10 \text{ km s}^{-1}$ (all errors quoted in this work are 1σ unless otherwise noted). This is in general agreement with, though slightly lower than, the H I systemic velocity derived by Cannon et al. (2004), $V_{\text{sys}} = 413 \pm 5 \text{ km s}^{-1}$. We note that our *FUSE* slit placement covers H I gas in emission at velocities from $\sim 405 - 415 \text{ km s}^{-1}$. Since velocity offsets of up to 20 km s^{-1} are common in *FUSE* spectra, we interpret the velocity centroid of the molecular gas to be coincident with the H I and stellar populations. We measure blueshifts of other species with respect to the velocity centroid for H_2 absorption, $v_{\text{H}_2} = 401 \pm 5 \text{ km s}^{-1}$.

We detect absorption lines of N, O, Si, P, Ar and Fe that arise from the neutral gas phase (i.e., ionization potentials greater than or near that of H). The velocity centroids of the strongest lines in clean spectral regions (including N I $\lambda 1134.980 \text{ \AA}$, N I $\lambda 1134.415 \text{ \AA}$, O I $\lambda 1039.230 \text{ \AA}$, Si II $\lambda 1020.699 \text{ \AA}$, P II $\lambda 1152.818 \text{ \AA}$, Ar I $\lambda 1048.220 \text{ \AA}$, Ar I $\lambda 1066.660 \text{ \AA}$,

Fe II λ 1096.877 Å, and Fe II λ 1063.176 Å) yield an average neutral gas velocity of $v_{\text{neutral}} = 392 \pm 10 \text{ km s}^{-1}$. This can be compared with the molecular gas velocity derived above, $v_{\text{sys}} = 401 \pm 10 \text{ km s}^{-1}$. These values are equal within the errors; the small offset between the two may be caused by the neutral gas being split into two kinematic components (separated by 10-20 km s^{-1}). To test for this, we compared fits for single and double Gaussian components to the strongest line profiles (including O I λ 1039.230 Å, Si II λ 1020.699 Å, and Fe II λ 1063.176 Å), but found no statistically significant difference (in χ^2 per degree of freedom) between them. The weakness of the putative second component introduces a negligible contribution to the error budgets for derived column densities and abundances (see below).

There are two ionized gas absorption lines detected in clean regions of our spectra, including the λ 1037.018 Å line of C II* and the λ 1012.495 Å line of S III. These absorptions give an average ionized gas velocity of $v_{\text{ionized}} = 377 \pm 9 \text{ km s}^{-1}$; i.e., offset with respect to the molecular gas by -24 km s^{-1} . Finally, coronal gas is detected in O VI λ 1031.926 Å absorption at a velocity of 370 km s^{-1} . This is blueshifted from the molecular gas velocity by -31 km s^{-1} , from the neutral gas by -22 km s^{-1} , and from the ionized gas by -7 km s^{-1} (though equal within errors). The weaker line of the doublet at λ 1037.617 Å falls in a complicated spectral region and is not used in the present analysis; see Figure 3 for a closer view of the spectral region around O VI. We present in Figures 4 and 5 the normalized line profiles of the detected absorption lines from the ISM of NGC 625 (absorption features were normalized by using clean spectral regions surrounding the lines; our error budget incorporates errors as a result of the continuum placements, which are usually comparable to the statistical noise).

This scenario is consistent with a low-velocity outflow, where the coronal gas has the largest velocity offset from the starburst region (which presumably is coincident with the velocity of the molecular and neutral gas absorption features). However, it is important to note that although the velocity centroids of the different types of gas may differ, there is considerable overlap in the velocity extents of many of the profiles (examine Figures 4 and 5). We interpret these changing velocity centroids and line breadths as results of the outflow, but it is clear that gas of all ionization levels co-exists throughout the galaxy. This velocity gradient is discussed further in § 4.1.

3.2. Column Densities

For each unblended spectral line shown in Table 2, the absorption profiles were converted into apparent optical depths, and then these profiles were integrated over velocity (see further discussion in Savage & Sembach 1991). The essence of this technique is to measure the depth

of normalized absorption lines as a function of velocity, and then to use atomic physics to infer the column density that best reproduces such a line profile. The column density and normalized line depth are related by:

$$N = \frac{m_e c}{\pi e^2 f \lambda} \int \ln \frac{I_0(v)}{I(v)} dv \quad (1)$$

where N is the column density in atoms cm^{-2} , m_e is the mass of the electron, c is the speed of light, e^2 is the standard unit of charge, f is the oscillator strength of the transition, λ is the rest wavelength of the transition, and $\ln \frac{I_0(v)}{I(v)}$ is the apparent optical depth as a function of velocity (the natural logarithm of the ratio of intensity in the continuum versus intensity in the line, as a function of velocity). This method is preferred over other common practices (e.g., curve of growth analysis) because it does not presume a functional form for the line under analysis. In general, the results from standard curve of growth techniques and the apparent optical depth method agree very well, and we adopt the apparent optical depth method values in this work. Note that the kinematic characteristics were derived separately using Gaussian fitting (see above).

For the diffuse molecular hydrogen absorption detected, we derive weighted mean column densities of $\log(N(\text{H}_2)) = 14.92 \pm 0.19$ ($J=0$), 14.91 ± 0.09 ($J=1$), and 14.47 ± 0.13 ($J=2$). Following Tumlinson et al. (2002), we can infer a range of rotational temperatures, T_{01} , of $\sim 70\text{-}90$ K. At high densities where collisions dominate the level populations, this value is indicative of the kinetic temperature of the gas. Such a progression is expected for relatively low-excitation H_2 , with the bulk of the diffuse gas in the lowest available rotational levels, and the column densities rapidly decreasing toward higher rotational levels. Derivation of the H I absorbing column is discussed in § 3.3; combining this estimate with the measured molecular columns implies a diffuse molecular fraction $f_{\text{H}_2} \sim 2 \times 10^{-5}$. It should be noted that this value samples the most UV-bright sightlines, and hence is heavily weighted toward material on the line of sight to the major starburst region. This is not coincident with the highest H I column density seen in emission (which is offset with respect to the starburst region; see Cannon et al. 2004) nor with a large detected molecular cloud (from CO observations; see Côté, Braine, & Cannon, in preparation). In general this highlights a shortcoming of the Lyman and Werner bands in probing cool molecular gas, as these lines are sensitive to diffuse gas (i.e., sightlines with low extinctions) but are less sensitive to the more common discrete molecular clouds and star formation complexes where the bulk of the cool molecular material is expected to reside (since these regions will be more heavily extinguished and hence have less background UV continuum emission). This point is discussed in more detail in § 4.2.

For other neutral and ionized gas absorption lines present in our spectra, we derive the following column densities: $\log(N) = 14.63$ (N I), 15.80 (O I), 15.37 (Si II), 13.54 (P II), 15.04 (S III), 13.98 (Ar I), and 14.73 (Fe II); typical errors are 0.1 - 0.2 dex (see Table 2). We note that the O I $\lambda 1039.230$ Å line may be saturated; since the SiC channels are of low S/N we cannot probe the amount of saturation empirically with other O lines in these data alone. We discuss tests for saturation and their implications in § 3.3. For the purposes of this paper, we adopt the empirical O I column (15.80 ± 0.12) as a lower limit; we note that this implies an upper limit for our implied neutral gas [N/O] ratio (see next section). For the coronal gas as traced by O VI $\lambda 1031.926$ Å absorption, we find $\log(N) = 14.32 \pm 0.08$. We use the neutral species to derive gas-phase abundances in the next subsection; the coronal gas is discussed in more detail in § 4.1.

3.3. Relative Gas-Phase Abundances

3.3.1. The Intrinsic H I Column

An estimate of the H I column density in NGC 625 from these data alone is hindered by the low S/N of the spectra in the SiC channels; this precludes us from using the higher-order Lyman lines, and we are left with only Ly β to constrain the H I column. However, the velocity separation of NGC 625 and the Milky Way and the low measured Galactic column along this high-latitude sightline (-73.1° ; we find a Galactic column $\log(N(\text{H I})) = 20.3 \pm 0.2$) are sufficient to clearly separate Galactic and intrinsic absorption profiles. This allows us to analyze both the red and blue wings of the NGC 625 H I absorption feature, better constraining our fit to the H I column density. We present in Figure 6 a closer view of the region surrounding Ly β , overlaid with fits to both the Galactic and intrinsic H I columns.

A pronounced uncertainty remains in our measured H I column due to the presence of strong stellar O VI P-Cygni profiles in the spectrum redward of Ly β (see Figure 6). These features result in an uncertainty in the adopted continuum in the region around Ly β . We adopt the mean of a “low” and “high” continuum placement, as shown in Figure 6. This leads us to estimate the intrinsic H I column in NGC 625 at $\log(N(\text{H I})) = 20.5 \pm 0.3$. This is at least half a dex lower than the H I 21 cm emission column density in this region; comparing the *FUSE* aperture placement (see Figure 1) with the $\sim 15''$ resolution H I column density map presented by Cannon et al. (2004), we find that the *FUSE* aperture is completely enclosed within the 10^{21} cm^{-2} contour. We believe that this estimate and associated uncertainty for the sight line probed are robust. Using the 21 cm value would result in a stronger Ly β profile than the other models shown in Figure 6 (see the dot-dash line corresponding to $\log(N(\text{H I})) = 21$). The difference between our absorption estimate and the 21 cm value could easily be

due to the much different solid angles probed by the two measurements (a size ratio of 2.2:1 exists between the H I emission beam and the solid angle of the *FUSE* MDRS aperture). We discuss the implications of this offset in H I absorbing column in more detail in § 4.

3.3.2. Neutral Gas Column Densities and Implied Abundances

Using these column density estimates and assuming that the observed absorption lines arise from the main elemental species in the neutral ISM, we find the following abundances and elemental ratios: $[N/H] = -1.80 \pm 0.34$; $[O/H] \geq -1.36 \pm 0.33$ (we stress again that the O I $\lambda 1039.230$ Å line may be saturated, and hence the lower limit is quoted; see further discussion in § 3.3.3); $[Ar/H] = -1.08 \pm 0.33$; $[Si/H] = -0.67 \pm 0.34$; $[Fe/H] = -1.22 \pm 0.34$; $\log(N/O) \leq -1.17 \pm 0.17$ ($[N/O] \geq -0.44 \pm 0.21$). These values use the updated solar abundances of Holweger (2001; N, Si, Fe) and Asplund et al. (2004; O), or the older standard values of Anders & Grevesse (1989; Ar). These abundances are summarized in Table 3. Note that a downward shift of the assumed H I column leads to increased abundances, and that an increase in N(H I) leads to a decrease in inferred metal abundance (specifically, if the H I column is a factor of 2 larger, as might be inferred from the 21 cm emission in this direction [see § 3.3.1], the derived abundances will be a factor of 2 lower than the quoted values). Also, the N/O abundance ratio assumes that the neutral gas components are co-spatial (i.e., that the ionization correction factor is negligible).

Keeping in mind the relatively large errors involved with these absorption line abundance measurements, and the points about potential line saturation discussed in § 3.3.3, these neutral gas values can be compared with the nebular abundances presented by Skillman et al. (2003b). Therein, for the major star formation region which dominates these *FUSE* sightlines, the calculated abundance ratios were found to be $[O/H] = -0.47 \pm 0.06$ and $\log(N/O) = -1.33 \pm 0.02$. Our neutral gas oxygen abundance (taken at face value) is found to be lower by ~ 0.9 dex, while the relative abundances between N and O are very similar. The offset between the neutral and nebular gas abundances may indicate that the outer regions of dwarf galaxies are less enriched in heavy elements compared to the inner, star-forming regions. We discuss this point further and compare to results found for other dwarf starbursts in the literature in § 4.3.

It is interesting to note that Skillman et al. (2003b) found an elevated N/O ratio in the three highest surface brightness H II regions in NGC 625 when compared to other star-forming dwarf galaxies. This value was found to be comparable to those for blue compact dwarfs, and was postulated to potentially arise as an effect of a long quiescent period prior to the current (temporally and spatially extended) star formation episode where the N abundance

may be elevated by the evolution of intermediate mass stars. Our neutral gas N/O ratio (which is equal to the nebular value, within errors) is also found to be high compared to the neutral N/O values derived for other dwarf starbursts observed with *FUSE* (note that if the O I λ 1039.230 Å line is saturated, the N/O value decreases, moving the NGC 625 N/O ratio closer to the values found for other systems). While interpretation of the elevated N/O ratio in the neutral gas of starbursting dwarfs will require a larger statistical sample, it appears that in NGC 625 the nucleosynthetic products of intermediate mass stars have been enriching the ISM for a long period, and that these products have been mixed into the neutral gas at large separations from the starburst regions (see also § 4.3).

3.3.3. *Effects of Potential Line Saturation*

As mentioned previously, the O I λ 1039.230 Å line may be saturated, potentially severely underestimating the true O I column density. As shown in Pettini & Lipman (1995), strongly saturated O I absorption lines can imply abundance ranges of up to ~ 1000 without differences in the goodness of the profile fit. Examining the profile of the O I line in Figure 5, it is clear that even this moderate-strength transition [$\log(f\lambda) = 0.974$] is close to saturation in the central regions of the line. Furthermore, since these *FUSE* data probe multiple sightlines (see Figure 1), the line may be more heavily saturated than the profile shows, if a luminous continuum source is not shielded by the foreground O I region. For these reasons, we more carefully explore the tests for, and potential effects of, O I line saturation.

We can probe the amount of line saturation by subtracting the local rms value from the line profile and re-deriving the column density via the apparent optical depth method. This exercise shows that the center of the line is within 1σ of zero flux; this causes the inferred column density to grow quickly (see Equation 1 and discussion in § 3.2). This suggests that the O I line is at least partially saturated.

The degree of this saturation can be tested by using tracer species to infer the column of neutral oxygen. First, Si II can be used as a proxy by assuming that the O/Si ratio is the same as the solar ratio (see Lu et al. 1998 for details). While uncertain, this method suggests that O I saturation may cause the O I column to be underestimated by as much as 0.7 dex. Note, however, that Si can be depleted onto dust grains, and thus this technique is not without error. Second, P II (which is less depleted onto dust grains) can be used as a tracer of the neutral oxygen abundance. Following Lebouteiller et al. (2004), if $[P/O] = 0$ is assumed for the neutral gas, then the implied column of O I is nearly a full dex above that derived from the actual O I line profile. Both of these proxy methods imply that the O I column has indeed been severely underestimated.

Ideally, one would use other oxygen lines in the SiC channels to independently test for line saturation. As mentioned previously, these data lack the S/N in the SiC channels to perform such a test. Thus, in lieu of a large sample of O/Si and P/O studies of the neutral ISM of dwarf galaxies, for the remainder of this paper we explore the results of a column of O I as derived above, $\log(N) = 15.80 \pm 0.12$, which implies an abundance offset when compared to the nebular regions. We discuss the implications of this scenario in § 4.3. We stress, however, that this O I column density is a lower limit and that the effects of line saturation may indeed be pronounced.

4. Discussion

The most important results in this paper are as follows: 1) The discovery of outflowing coronal gas from a relatively low-luminosity dwarf starburst galaxy; 2) The discovery of diffuse H₂ absorption in a relatively distant, low-metallicity galaxy; 3) The discovery of a possible abundance offset between the nebular and neutral gas phases in a star-forming dwarf galaxy. In this section we discuss each of these points in more detail and compare the values found for NGC 625 with those found for other dwarf starbursts in the literature.

4.1. Outflowing Coronal Gas

The coronal gas content of low-mass systems that are undergoing outflow episodes is an important component of models of superbubble evolution. If the coronal gas density is high and radiative cooling is efficient, then outflow energies can be expended prior to the outflow breaking out of the disk and venting hot gas, metals and energy into the surrounding IGM. If, on the other hand, the coronal gas density is low and the radiative cooling is inefficient, then the coronal gas does not radiate sufficient energy to slow or stall galactic-scale outflows from low-mass galaxies. While the evolution of outflows is complex and depends on various other factors, coronal gas cooling is one important effect that has only recently become accessible observationally.

In principal, by observing the absorption and emission profiles of outflowing O VI gas from a galaxy, one can obtain an estimate of the cooling rate of the gas and compare this to the estimated energy input into the ISM by the evolution of the massive stars associated with recent star formation (see Heckman et al. 2001). However, such an estimate of the cooling rate in NGC 625 is difficult for two reasons. First, it is not straightforward to extrapolate to an unambiguous outflow cavity size estimate. Second, the low outflow velocity of the O VI

gas with respect to the molecular gas (and presumably the stellar population) in NGC 625 ($\sim 30 \text{ km s}^{-1}$) does not cleanly separate the absorption profile from the expected location of O VI emission (if we see emission only from the redshifted, back side of a symmetric outflow along the line of sight). These factors complicate estimates of the mass and density of the O VI gas, both of which are needed to constrain the cooling rate (see Shull & Slavin 1994).

FUSE observations of O VI emission from other starbursting galaxies have shown that typical cooling rates in coronal gas are small. Heckman et al. (2001) and Hoopes et al. (2003) estimate that coronal gas cooling is roughly comparable to the energy radiated away in soft x-ray emission in the outflows in NGC 1705 and M 82. Since the soft x-ray emission radiates only a small fraction of the input energy of the wind (Strickland & Stevens 2000), the cooling rate via coronal gas appears to be small. A similar column of O VI gas has been found in NGC 625 ($\log(N(\text{O VI})) = 14.32 \pm 0.08$) and NGC 1705 ($\log(N(\text{O VI})) = 14.26 \pm 0.08$); because the outflow cavity is likely smaller in NGC 625 than in NGC 1705 (implying a smaller mass of cooling plasma), it is likely that radiative cooling via coronal gas is not a significant portion of the energy budget of NGC 625.

Comparing to the literature, it appears that pronounced O VI absorption is ubiquitous in actively star-forming systems with non-zero inclinations. Extensive observations through the Milky Way halo have shown an average O VI absorption column density of 14.38 (Savage et al. 2003). Similarly, Howk et al. (2002) and Hoopes et al. (2002) have shown that O VI absorption is present along tens of sightlines into the Large and Small Magellanic Clouds, with average column densities of 14.37 and 14.53, respectively. Finally, studies of extragalactic dwarf systems with strong current star formation show at least weak O VI absorption when the major exciting clusters are observed directly (see Heckman et al. 2001 for NGC 1705; Lebouteiller et al. 2004 for I Zw 36; the present work for NGC 625). A large sample of *FUSE* dwarf galaxy observations spanning a range of galaxy properties (star formation rate, outflow velocities, dust content, etc.) is needed to quantify the importance of O VI in the cooling portions of the outflows.

4.2. Diffuse Molecular Gas

Diffuse H_2 is a ubiquitous component of the ISM of the Galaxy. Using *Copernicus* data, Savage et al. (1977) demonstrated a strong correlation between H I column or reddening and the presence of diffuse H_2 , with molecular gas usually found on sightlines with sufficient H I to allow self-shielding or sufficient dust to allow the efficient formation of H_2 . However, these early observations were limited to local sightlines due to instrumental limitations. The higher sensitivity of *ORFEUS* allowed H_2 to be studied in the Magellanic Clouds (see, e.g., de Boer

et al. 1998; Richter et al. 1998). Most recently, *FUSE* has greatly expanded the amount of observational data available on diffuse H₂. However, even though *FUSE* offers unprecedented spectral resolution and sensitivity (typical observations probe H₂ column densities $\sim 10^{15}$ cm⁻²), there have remained few detections of H₂ in extragalactic environments. Within the Local Group, diffuse H₂ has only been detected in the Milky Way (see, e.g., Shull et al. 2000 and numerous other studies), the Magellanic Stream (Richter et al. 2001; Sembach et al. 2001), the Magellanic Clouds (Tumlinson et al. 2002), and M 33 (Bluhm et al. 2003). As mentioned in § 1, extragalactic detections of diffuse H₂ beyond the Local Group are even more rare.

Dwarf starburst galaxies such as NGC 625 offer a unique opportunity to study diffuse H₂ in the ISM, since they are typically UV-bright, are forming stars rapidly (implying a sizable molecular reservoir), and usually present relatively low extinctions due to their low metal abundances. Even with these apparent observational advantages, however, stringent column density limits of $\log(N(\text{H}_2)) < 15$ in the low-J levels are derived for the metal-deficient starburst galaxies I Zw 18 (Vidal-Madjar et al. 2000), NGC 1705 (Heckman et al. 2001), Mrk 59 (Thuan et al. 2002) and I Zw 36 (Lebouteiller et al. 2004). The new sample of Hoopes et al. (2004) also searches for diffuse H₂ gas in NGC 3310, NGC 4214, M 83, and NGC 5253; only M 83 and NGC 5253 show detectable H₂ gas in absorption against the background UV continuum of the massive stellar populations.

Hoopes et al. (2004) interpret the low molecular fractions derived in their sample (typically $f_{\text{H}_2} \lesssim 10^{-5}$; i.e., similar to the fraction found in the present study for NGC 625) to the stronger UV radiation fields of these galaxies. This stronger UV background will raise the minimum values of extinction and H I column necessary for diffuse H₂ to remain in the ISM without being destroyed. They also note that some of the systems in their sample have been detected in CO tracer lines and that the inferred molecular masses exceed the derived diffuse H₂ masses by many orders of magnitude.

The detection of H₂ absorption in NGC 625 highlights the importance of ISM geometry in the interpretation of these types of observations. As shown by Cannon et al. (2002), the dust distribution (and hence potentially productive areas of H₂ formation) does not always follow the distribution of UV light. This implies that UV absorption experiments for diffuse H₂ may not sample the sightlines expected to show the highest columns of molecular gas. In the case of NGC 625, we have a combination of sightlines into a moderately dusty starburst region (extinctions toward the massive clusters of up to ~ 1 magnitude in the V-band; see Cannon et al. 2003) that has a moderate UV radiation field (since no higher-level H₂ transitions are detected). Here, the potential for detection of H₂ may be optimized, given the correlation between dust and H₂ (see, e.g., Savage et al. 1977).

The simplest interpretation of these H₂ observations of nearby dwarf starburst and low-metallicity galaxies appears to be one where the covering factor of diffuse H₂ clouds is low. This implies that most of the molecular material is confined to relatively small, dense molecular clouds, as predicted in models of the low-metallicity ISM (see, e.g., Maloney & Black 1988; Norman & Spaans 1997; Pak et al. 1998; Bolatto et al. 1999). Since the strength of the UV radiation field appears to be an important factor both theoretically and observationally, it may be expected that sightlines to the UV-brightest clusters may not show diffuse H₂ in absorption. The complicated geometry of dust, neutral and molecular gas, and the current stellar populations will require a much larger sample to fully understand the nature of diffuse H₂ absorption in extragalactic environments.

4.3. Abundances in the Neutral and Nebular Gas

In these data we find an apparent abundance difference between the neutral and nebular gas regions in NGC 625. Interestingly, the N/O ratio is, within errors, identical in the neutral and nebular gas phases. We again emphasize that our O I λ 1039.230 Å line may be saturated (hence reducing the offset between N and O abundances), and that our absolute abundances are comparatively uncertain due to the large error on our measured H I column within NGC 625. However, taken at face value, the offset is large enough (~ 0.9 dex) to warrant a more thorough discussion of these values in other systems and the potential implications for the evolution of low-mass galaxies.

As shown in Table 3, it appears that such abundance offsets between nebular and neutral gas are common in strongly star-forming dwarf galaxies studied to date with *FUSE*. Abundance differences of > 0.5 dex have been found in NGC 1705 (Heckman et al. 2001), IZw 18 (Aloisi et al. 2003; but see also Lecavelier des Etangs et al. 2004 for an alternative treatment), IZw 36 (Lebouteiller et al. 2004), and Mrk 59 (Thuan et al. 2002). These abundance differences may be caused by *FUSE* sightlines sampling two different components of the ISM of dwarf galaxies: lower-abundance halo gas, and higher-abundance gas nearer to the active star formation regions.

A simple test of this “disk vs. halo” scenario can be performed by comparing the size of the abundance difference with the difference between the H I gas column seen in emission and the H I column that can only be foreground to the UV-luminous regions (i.e., the H I gas probed in *FUSE* observations). Our reasoning is simple: if the absorption arises in the disk of the galaxy, the column density should be comparable to the disk column density, but if the absorption arises in a halo, the column density should be smaller. We show in Figure 7 a plot of the size of the offset between neutral and nebular gas ($\Delta([O/H]) = [O/H]_{\text{neutral}} -$

$[O/H]_{\text{nebular}}$) and the difference in H I columns as seen in absorption and in emission toward the same region ($\Delta(\text{H I}) = \log(N(\text{H I}))_{\text{FUSE}} - \log(N(\text{H I}))_{21\text{ cm}}$). Depending on the value chosen for IZw 18, there could be a trend of increasing $\Delta([O/H])$ with increasing $\Delta(\text{H I})$. It appears that each system under study (with the possible exception of IZw 18) shows some value of abundance offset between the nebular and neutral gas (see notes to Table 3 for more details). Each of these investigations is susceptible to various sources of error that will require a larger sample to overcome; however, if these results are supported by further data, it appears that many dwarf galaxies may have a halo of lower-metallicity gas that surrounds the actively star-forming regions as probed by emission line spectroscopy.

This result has important implications for the chemical evolution of star-forming dwarf galaxies, since it implies that widespread enrichment episodes have preceded the current bursts that dominate the bolometric luminosity of these systems. Previous works have postulated a prompt “self-enrichment” scenario in the nebular gas region that would be evidenced by localized enrichment near current H II regions (e.g., Kunth & Sargent 1986). This effect has been shown to be small, since local abundance variations are not seen in the nebular regions surrounding massive starbursts in low-mass galaxies (see Kobulnicky & Skillman 1996, Kobulnicky & Skillman 1997, Kobulnicky et al. 1997, Kobulnicky & Skillman 1998, Legrand et al. 2000, and references therein).

The present offset between neutral and nebular gas abundances would require a different enrichment scenario than “localized enrichment”, since the absorbing columns are, by definition, foreground to the starburst regions. A potential scenario that would be consistent with these data is one where low-level star formation persists in dwarf galaxies for extended periods of time, allowing the oxygen and nitrogen abundances to be elevated in the ISM and efficiently mixed with the surrounding neutral gas. This low-level star formation rate would elevate the neutral gas abundances above the primordial value, and the higher nebular values could then be produced by more recent star formation in the current major star formation regions of these systems. The close agreement in N/O between the nebular and neutral gas also points toward central creation and geometrical dilution over a long time period; otherwise the different production timescales for N and O become problematic. A larger *FUSE* sample of actively star forming dwarf galaxies would be most beneficial in addressing the abundance offsets between nebular and neutral gas phases.

If the absorption spectra of dwarf galaxies obtained by *FUSE* are indeed sampling a halo of neutral gas and are not primarily produced in the disks, then they provide a very important probe of a virtually unstudied component of the dwarf galaxy ISM. Kennicutt & Skillman (2001) have emphasized the importance of measuring abundances in the neutral gas in the outer parts of dwarf galaxies. In spiral galaxies, it is well known that there are

chemical abundance gradients in the sense of lower abundances in the outer parts of the systems. However, in dwarf galaxies it is generally assumed that the entire H I disk has the same metallicity as measured in the H II regions, and this is a very uncertain assumption. The physical basis for this assumption is the general uniformity of H II region abundances in dwarf galaxies (Kobulnicky & Skillman 1997 and references therein), and the inference that the whole H I disk is kept at a rather uniform chemical abundance by the rapid transportation of the metals in a hot phase of the ISM (Clayton & Pantelaki 1993; Tenorio-Tagle 1996). However, the H II regions only sample the inner parts of the H I disk. In some dwarf galaxies, as much as 90% of the neutral hydrogen lies outside of the Holmberg radius (e.g., DDO 154; Carignan & Freeman 1988; Carignan & Purton 1998). If dwarf galaxies do have chemical abundance gradients, then assuming that the chemical abundances are constant overestimates the total metal content of the galaxy, and leads to a misinterpretation of their evolutionary status (e.g., artificially inflating the calculated effective yield). The edge-on orientation of NGC 625 implies that at least some of the absorption is occurring in the outer parts of the galaxy and thus providing a probe of this relatively unexplored ISM component.

The extended mission of *FUSE* offers an ideal opportunity to test for this important evolutionary scenario. One would ideally seek a sample of luminous, metal-poor ($\lesssim 10\% Z_{\odot}$) dwarf systems that have low intrinsic H I foreground columns, low foreground and internal extinctions, along high-visibility sightlines not contaminated by intermediate- or high-velocity clouds. Deep integrations on such targets will provide sufficient S/N to allow inter-comparison of the columns derived from oxygen lines with different oscillator strengths throughout the *FUSE* spectral region. With the effects of line saturation eliminated, such a sample would allow the exploration of this potentially important ISM phase in dwarf galaxies.

5. Conclusions

We have presented new *FUSE* spectroscopy of the dwarf starburst galaxy NGC 625. These data allow a detailed investigation of multiple phases of the ISM of the galaxy, including the molecular, neutral, ionized and coronal gas contents. We use these data to study the kinematics of the ISM, the diffuse H₂ content, and the abundances in the neutral gas phase.

Our first major result is that O VI absorption has been detected in a relatively low-velocity outflow. This detection adds to the sample of extragalactic systems showing outflowing coronal gas. With these data alone we cannot constrain the efficiency of cooling in the coronal gas; however, comparing to the literature and given the strength of the O VI absorption feature, we suggest that radiative cooling is likely not a dominant mechanism in the loss of energy from the NGC 625 outflow.

Our second major result is that we have detected low rotational level transitions from the Lyman and Werner bands of diffuse H_2 gas in NGC 625. This is one of only a few dwarf galaxies outside of the Local Group to show diffuse H_2 in *FUSE* observations. It is likely that the geometry of the stellar populations, dust, neutral and dense molecular gas all play a role in determining if H_2 is detectable in such systems. We interpret the low molecular fraction, which is similar to that found in other dwarf starburst and low-metallicity galaxies from *FUSE* studies, to the low covering factor of H_2 clouds, which are expected to be comparatively small and dense in these actively star-forming, metal-deficient environments.

Our final important result is that we have found a potential abundance offset between the nebular and neutral gas phases of NGC 625. While the absolute oxygen abundance is hindered by potential saturation and the intrinsic H I column is only constrained to ± 0.3 dex, the magnitude of the offset (~ 0.9 dex) suggests that it is likely real. Interestingly, the N/O ratio is found to be the same in both the nebular and neutral phases. Similar results have been found for other dwarf galaxies studied with *FUSE*, suggesting that dwarf galaxies may in general host a lower-metallicity halo of neutral gas that can only be probed by absorption line spectroscopy. A larger sample of systems will help to shed light on this important evolutionary scenario.

We thank Max Pettini for several valuable comments including insights into aspects of oxygen line saturation; S. R. McCandliss for making the *H₂ools* package available; and Henry Lee & Simon Strasser for helpful discussions. We are also grateful to the anonymous referee for a careful reading of this manuscript and numerous helpful comments. J.M.C. was supported by NASA Graduate Student Researchers Program (GSRP) Fellowship NGT 5-50346. E.D.S. is grateful for partial support from NASA LTSARP grant NAG5-9221 and the University of Minnesota. This research has been supported by NASA grant NNG 04GD25G. This research has made use of the NASA/IPAC Extragalactic Database (NED) which is operated by the Jet Propulsion Laboratory, California Institute of Technology, under contract with the National Aeronautics and Space Administration, and NASA's Astrophysics Data System.

REFERENCES

- Anders, E. & Grevesse, N. 1989, *Geochim. Cosmochim. Acta*, 53, 197
- Aloisi, A., Savaglio, S., Heckman, T. M., Hoopes, C. G., Leitherer, C., & Sembach, K. R. 2003, *ApJ*, 595, 760
- Asplund, M., Grevesse, N., Sauval, A. J., Allende Prieto, C., & Kiselman, D. 2004, *A&A*, 417, 751
- Bluhm, H., de Boer, K. S., Marggraf, O., Richter, P., & Wakker, B. P. 2003, *A&A*, 398, 983
- Bolato, A. D., Jackson, J. M., & Ingalls, J. G. 1999, *ApJ*, 513, 275
- Bomans, D. J. & Grant, M.-B. 1998, *Astronomische Nachrichten*, 319, 26
- Cannon, J. M., Skillman, E. D., Garnett, D. R., & Dufour, R. J. 2002, *ApJ*, 565, 931
- Cannon, J. M., Dohm-Palmer, R. C., Skillman, E. D., Bomans, D. J., Côté, S., & Miller, B. W. 2003, *AJ*, 126, 2806
- Cannon, J. M., McClure-Griffiths, N. M., Skillman, E. D., & Côté, S. 2004, *ApJ*, 607, 274
- Cannon, J. M. & Skillman, E. D. 2004, *ApJ*, 610, 772
- Carignan, C. & Freeman, K. C. 1988, *ApJ*, 332, L33
- Carignan, C. & Purton, C. 1998, *ApJ*, 506, 125
- Clayton, D. D. & Pantelaki, I. 1993, *Phys. Rep.*, 227, 293
- Conti, P. S. 1991, *ApJ*, 377, 115
- de Boer, K. S., Richter, P., Bomans, D. J., Heithausen, A., & Koornneef, J. 1998, *A&A*, 338, L5
- Dufour, R. J. 1984, *IAU Symp. 108: Structure and Evolution of the Magellanic Clouds*, 108, 353
- Garnett, D. R. 1999, *IAU Symp. 190: New Views of the Magellanic Clouds*, 190, 266
- Heckman, T. M., Sembach, K. R., Meurer, G. R., Strickland, D. K., Martin, C. L., Calzetti, D., & Leitherer, C. 2001, *ApJ*, 554, 1021
- Holweger, H. 2001, *AIP Conf. Proc. 598: Joint SOHO/ACE workshop "Solar and Galactic Composition"*, 598, 23

- Hoopes, C. G., Heckman, T. M., Strickland, D. K., & Howk, J. C. 2003, *ApJ*, 596, L175
- Hoopes, C. G., Sembach, K. R., Heckman, T. M., Meurer, G. R., Aloisi, A., Calzetti, D., Leitherer, C., & Martin, C. L. 2004, *ApJ*, in press
- Hoopes, C. G., Sembach, K. R., Howk, J. C., Savage, B. D., & Fullerton, A. W. 2002, *ApJ*, 569, 233
- Howk, J. C., Sembach, K. R., Savage, B. D., Massa, D., Friedman, S. D., & Fullerton, A. W. 2002, *ApJ*, 569, 214
- Izotov, Y. I. & Thuan, T. X. 1999, *ApJ*, 511, 639
- Kennicutt, R. C. & Skillman, E. D. 2001, *AJ*, 121, 1461
- Kobulnicky, H. A. & Skillman, E. D. 1996, *ApJ*, 471, 211
- Kobulnicky, H. A. & Skillman, E. D. 1997, *ApJ*, 489, 636
- Kobulnicky, H. A. & Skillman, E. D. 1998, *ApJ*, 497, 601
- Kobulnicky, H. A., Skillman, E. D., Roy, J., Walsh, J. R., & Rosa, M. R. 1997, *ApJ*, 477, 679
- Kunth, D. & Sargent, W. L. W. 1986, *ApJ*, 300, 496
- Lee, H., & Skillman, E. D. 2004, *ApJ*, in press (astro-ph/0406571)
- Lebouteiller, V., Kunth, D., Lequeux, J., Lecavelier des Etangs, A., Désert, J.-M., Hébrard, G., & Vidal-Madjar, A. 2004, *A&A*, 415, 55
- Lecavelier des Etangs, A., Désert, J.-M., Kunth, D., Vidal-Madjar, A., Callejo, G., Ferlet, R., Hébrard, G., & Lebouteiller, V. 2004, *A&A*, 413, 131
- Legrand, F., Kunth, D., Roy, J.-R., Mas-Hesse, J. M., & Walsh, J. R. 2000, *A&A*, 355, 891
- Lu, L., Sargent, W. L. W., & Barlow, T. A. 1998, *AJ*, 115, 55
- Mac Low, M. & Ferrara, A. 1999, *ApJ*, 513, 142
- Maloney, P. & Black, J. H. 1988, *ApJ*, 325, 389
- Marlowe, A. T., Meurer, G. R., Heckman, T. M., & Schommer, R. 1997, *ApJS*, 112, 285
- Meurer, G. R., Staveley-Smith, L., & Killeen, N. E. B. 1998, *MNRAS*, 300, 705

- McCandliss, S. R. 2003, *PASP*, 115, 651
- Moos, H. W., et al. 2000, *ApJ*, 538, L1
- Morton, D. C. 2003, *ApJS*, 149, 205
- Norman, C. A. & Spaans, M. 1997, *ApJ*, 480, 145
- Pak, S., Jaffe, D. T., van Dishoeck, E. F., Johansson, L. E. B., & Booth, R. S. 1998, *ApJ*, 498, 735
- Pettini, M. & Lipman, K. 1995, *A&A*, 297, L63
- Richter, P., et al. 1998, *A&A*, 338, L9
- Richter, P., Sembach, K. R., Wakker, B. P., & Savage, B. D. 2001, *ApJ*, 562, L181
- Savage, B. D., Drake, J. F., Budich, W., & Bohlin, R. C. 1977, *ApJ*, 216, 291
- Savage, B. D. & Sembach, K. R. 1991, *ApJ*, 379, 245
- Savage, B. D., et al. 2003, *ApJS*, 146, 125
- Sembach, K. R., Howk, J. C., Savage, B. D., & Shull, J. M. 2001, *AJ*, 121, 992
- Schaerer, D., Contini, T., & Kunth, D. 1999, *A&A*, 341, 399
- Schlegel, D. J., Finkbeiner, D. P., & Davis, M. 1998, *ApJ*, 500, 525
- Shull, J. M. & Slavin, J. D. 1994, *ApJ*, 427, 784
- Shull, J. M., et al. 2000, *ApJ*, 538, L73
- Skillman, E. D., Côté, S., & Miller, B. W. 2003a, *AJ*, 125, 593
- Skillman, E. D., Côté, S., & Miller, B. W. 2003b, *AJ*, 125, 610
- Skillman, E. D. & Kennicutt, R. C. 1993, *ApJ*, 411, 655
- Stil, J. M. & Israel, F. P. 2002, *A&A*, 389, 42
- Strickland, D. K. & Stevens, I. R. 2000, *MNRAS*, 314, 511
- Sutherland, R. S. & Dopita, M. A. 1993, *ApJS*, 88, 253
- Taylor, C. L., Kobulnicky, H. A., & Skillman, E. D. 1998, *AJ*, 116, 2746

Tenorio-Tagle, G. 1996, *AJ*, 111, 1641

Thuan, T. X., Lecavelier des Etangs, A., & Izotov, Y. I. 2002, *ApJ*, 565, 941

Tumlinson, J., et al. 2002, *ApJ*, 566, 857

van Zee, L., Westpfahl, D., Haynes, M. P., & Salzer, J. J. 1998, *AJ*, 115, 1000

Vidal-Madjar, A., et al. 2000, *ApJ*, 538, L77

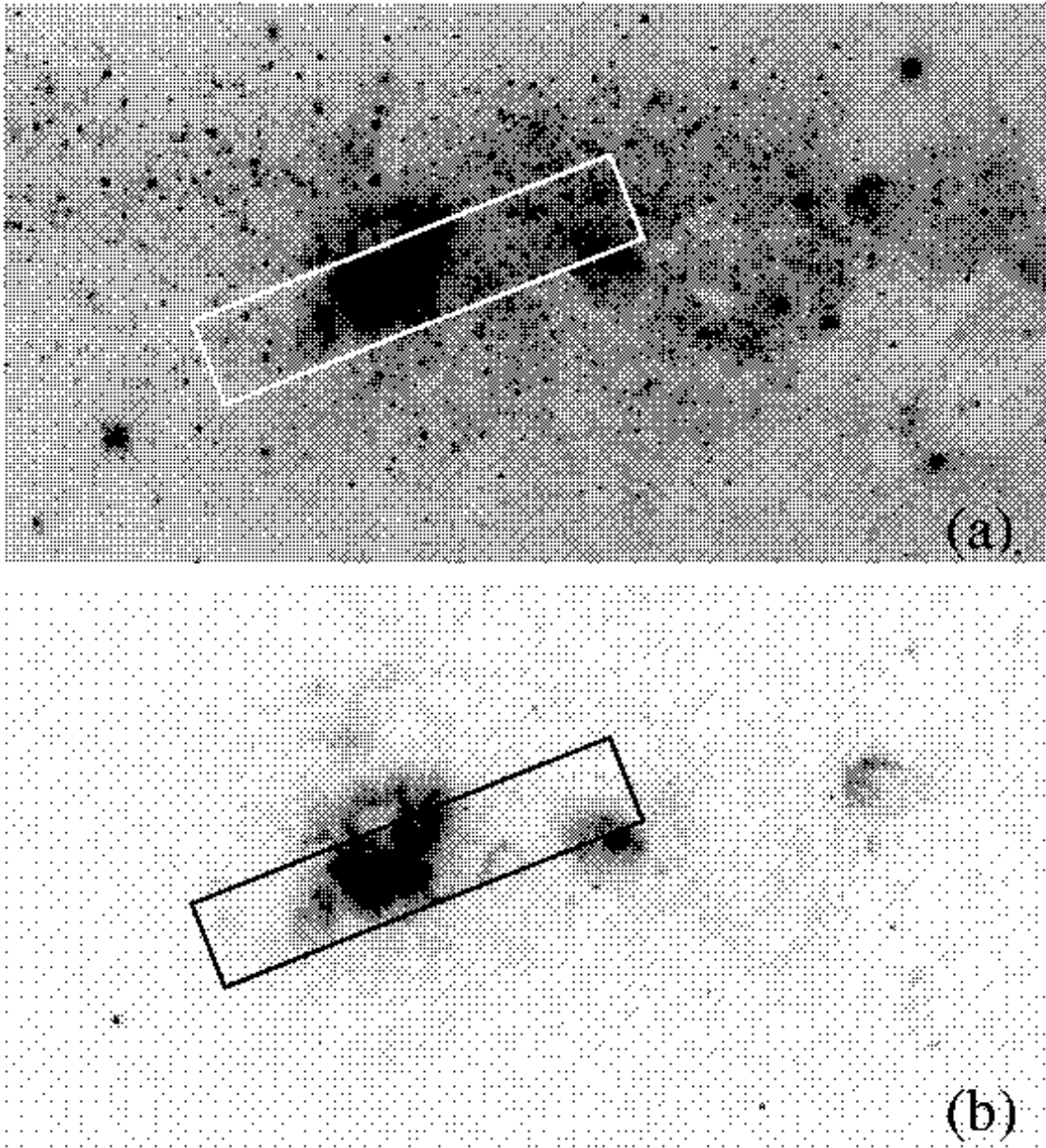


Fig. 1.— Position of the LiF1 detector segment of the *FUSE* MDRS $4'' \times 20''$ aperture overlaid on an *HST*/WFPC2 V-band image (a) and on an *HST*/WFPC2 continuum-subtracted $H\alpha$ image (b). The field of view is $\sim 875 \times 471$ pc at the distance of 3.89 Mpc, with north up and east to the left. The average position angle during these observations was 112° east of north, as shown. We estimate the positional accuracy of the slit to be $\pm 1''$, based on the nominal *FUSE* pointing accuracy ($\sim 0.5''$ rms), the *HST*/WFPC2 pointing accuracy ($\sim 0.5''$ rms) and the comparison to ground-based astrometric solutions. This slit placement is sensitive to the bulk of the UV flux from NGC 625.

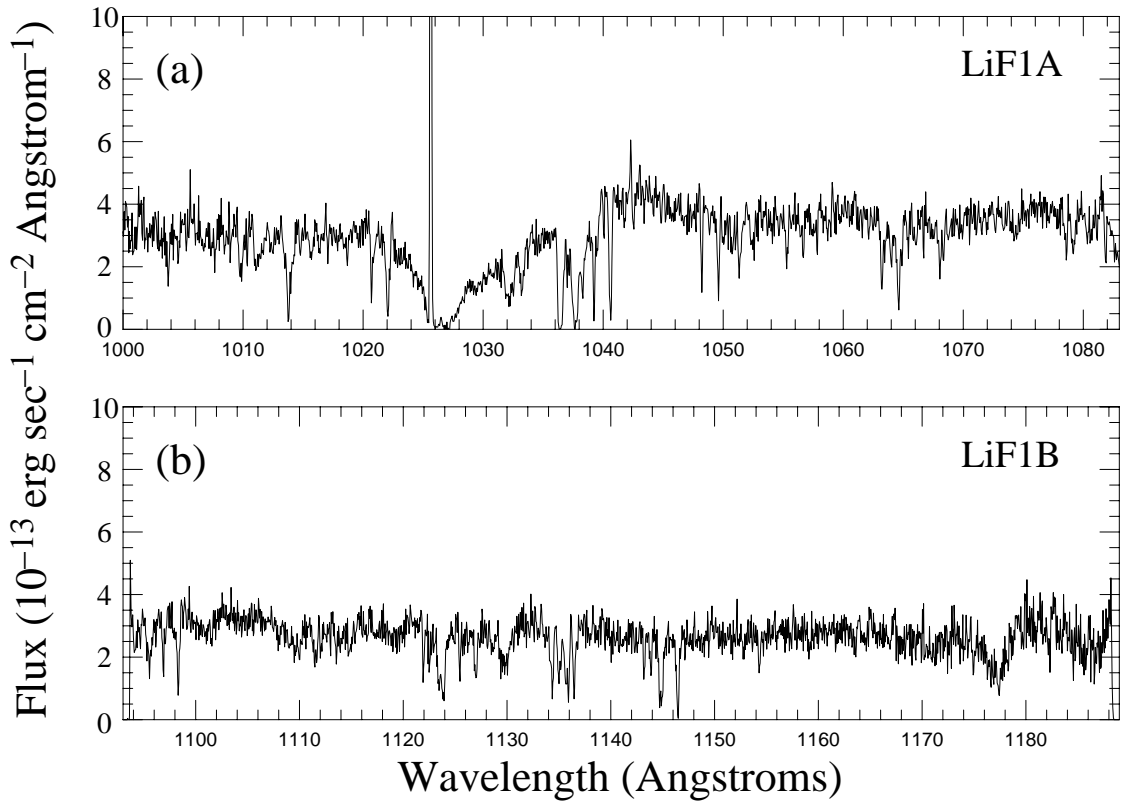


Fig. 2.— Overview of our *FUSE* spectra, with the LiF1A spectrum shown in (a) and the LiF1B spectrum shown in (b). These data have been binned by 8 pixels (~ 0.05 Å) for clarity. Note the numerous absorption lines detected throughout this spectral region.

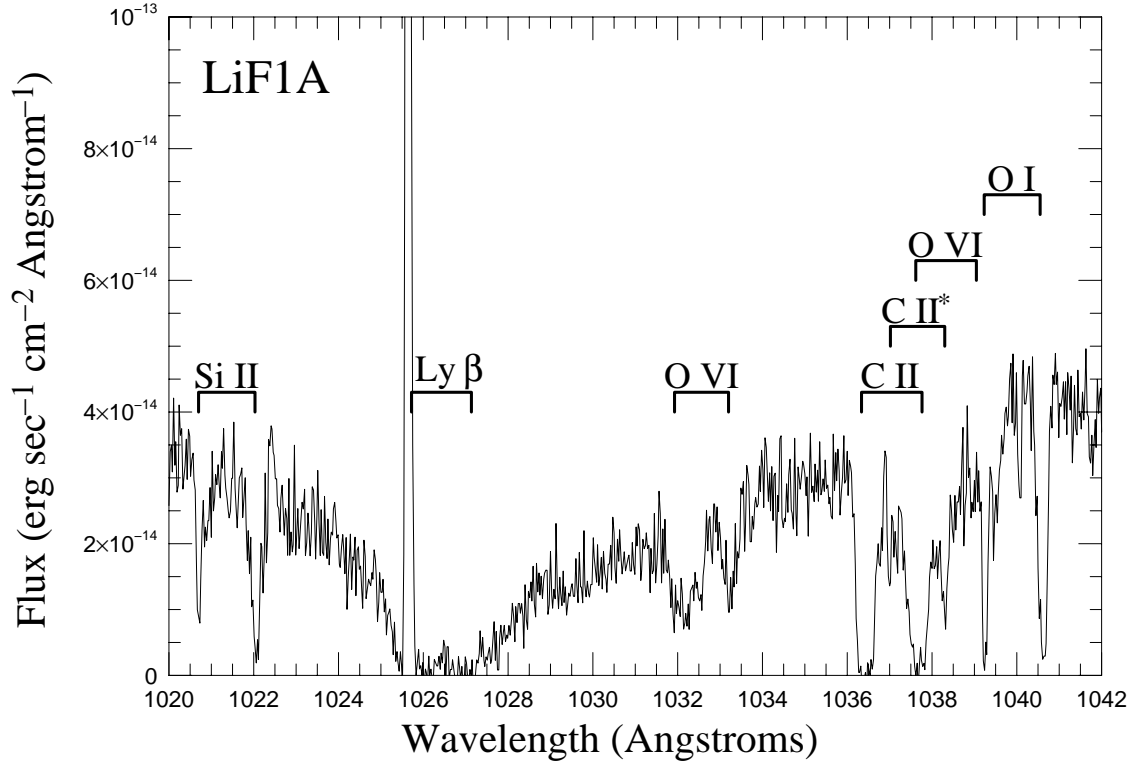


Fig. 3.— Closer view of the spectral region surrounding $\text{Ly}\beta$ and the O VI absorption features, from the LiF1A detector segment. Prominent absorption lines are labeled with both the Milky Way and NGC625 (systemic) velocities. The O VI absorption is strong (equivalent width $\sim 0.2 \text{ \AA}$) and the velocity centroid is blueshifted with respect to the molecular and neutral gas absorption centroids. See further discussion in § 3.1, and also Figures 4 and 5.

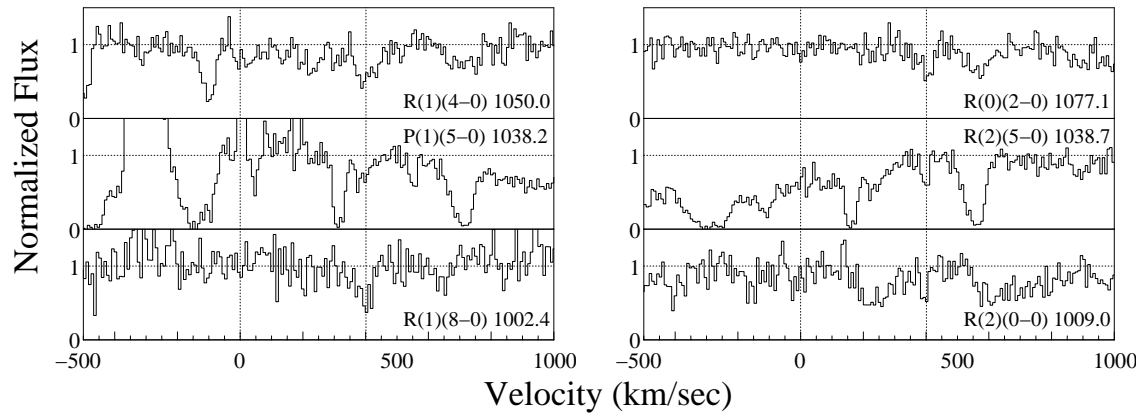


Fig. 4.— Normalized line profiles of identified H₂ lines arising within the ISM of NGC 625. Vertical lines show Milky Way and NGC 625 velocities; these H₂ lines are discussed further in §§ 3.1 and 3.2.

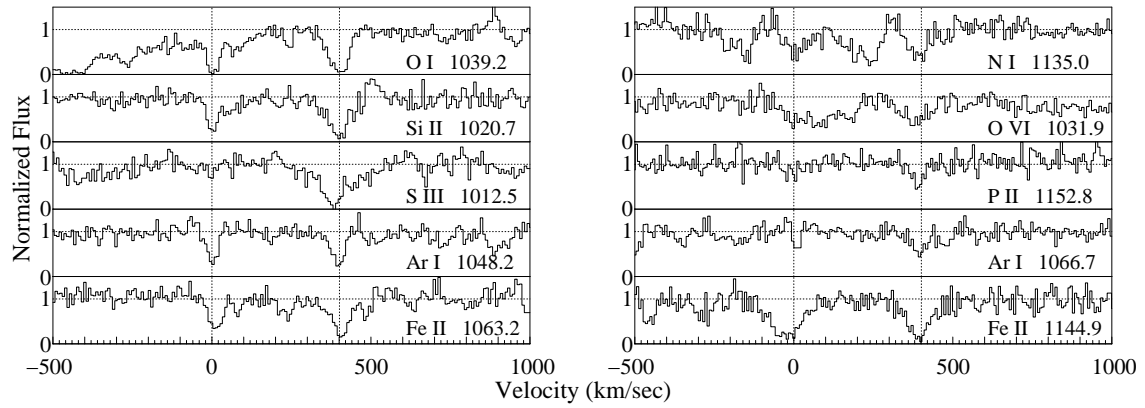


Fig. 5.— Normalized line profiles of identified neutral and ionized atomic absorption lines arising within the ISM of NGC 625. Vertical lines show Milky Way and NGC 625 velocities; these absorption lines are discussed further in §§ 3.1 and 3.2.

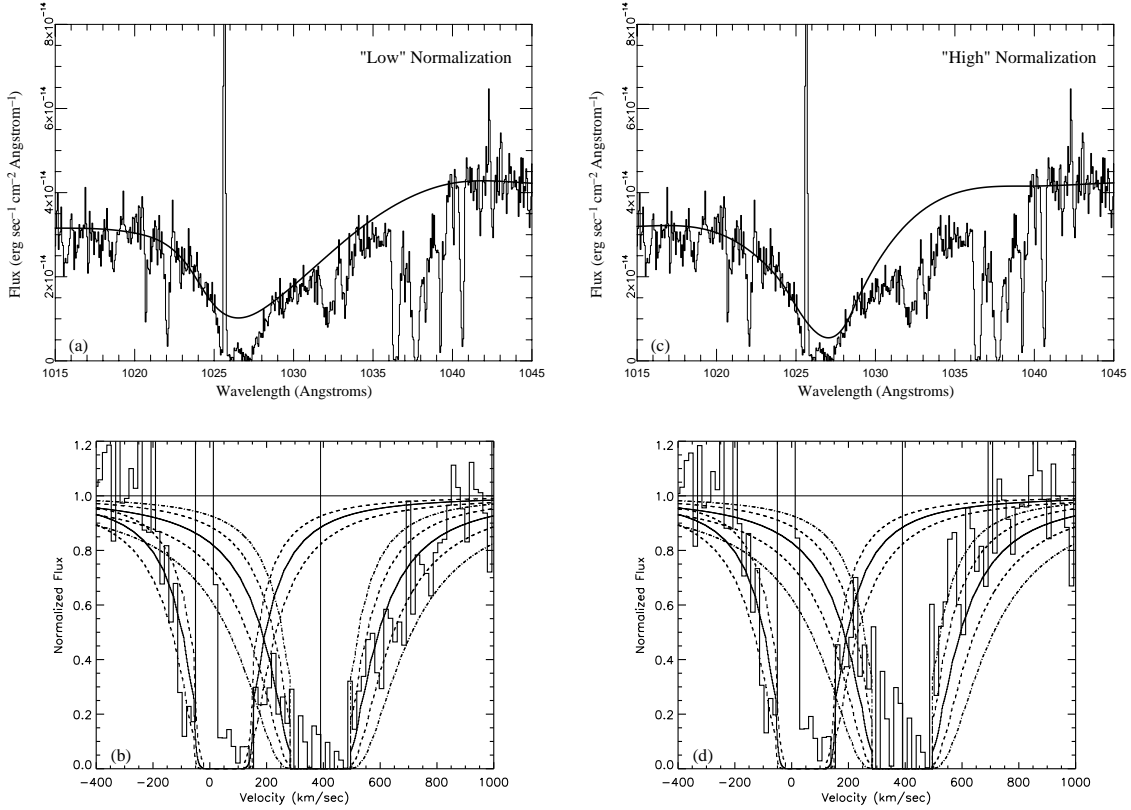


Fig. 6.— Profiles of Galactic and NGC 625 H I Ly β absorption. (a) and (c) show the “low” and “high” continuum normalizations, and (b) and (d) show the resulting H I absorption profiles. Overlaid on (b) and (d) are profiles for the Galactic and NGC 625 H I Ly β absorption. For the Milky Way profile, three lines are shown at $\log(N(\text{H I})) = 20.3$ (solid line) and $\log(N(\text{H I})) = 20.1, 20.5$ (dotted lines). For NGC 625, five lines are shown at $\log(N(\text{H I})) = 20.6$ (solid), $\log(N(\text{H I})) = 20.4, 20.8$ (dotted lines), and $\log(N(\text{H I})) = 20.2, 21.0$ (dot-dash lines). From these profiles we deduce an absorbing H I column of $\log(N(\text{H I})) = 20.5 \pm 0.3$ for NGC 625, with the continuum normalization dominating the error budget. See § 3.3 for further discussion.

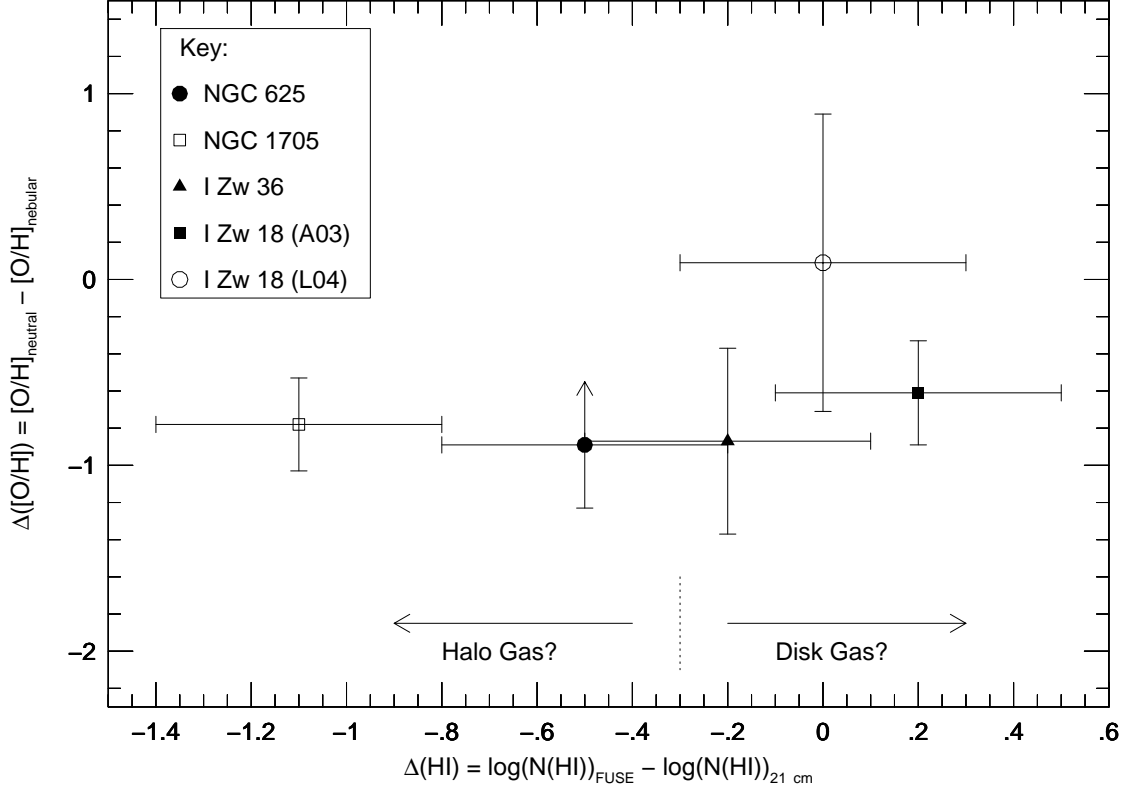


Fig. 7.— Differences between neutral and nebular gas abundances plotted versus the difference between H I absorption column density as probed by *FUSE* observations and H I 21 cm emission column density, for 4 different dwarf starburst galaxies. In the key, A03 corresponds to the study of Aloisi et al. (2003), and L04 corresponds to the study of Lecavelier des Etangs et al. (2004). Errorbars on $\Delta(\text{H I})$ are difficult to estimate, and are shown at the 0.3 dex level. We find no obvious correlation between these two values; rather, abundance offsets between the neutral and nebular gas appear to be common in the dwarf galaxies shown here. To the left of the dotted vertical line at $\Delta(\text{H I}) = -0.3$, one expects to probe “halo” gas via absorption line spectroscopy; to the right of this line, one expects only to probe gas close to the background sources within the disk.

Table 1. Basic Parameters of NGC 625

Property	Value	Reference
Distance (Mpc)	3.89 ± 0.22	Cannon et al. (2003)
M_B	-16.3	Marlowe et al. (1997)
b, l^a	$273.7^\circ, -73.1^\circ$	--
E(B-V)	0.016	Schlegel et al. (1998)
$12 + \log(\text{O}/\text{H})$	8.14 ± 0.02	Skillman et al. (2003b)
Current SFR ($M_\odot \text{ yr}^{-1}$)	0.05	Skillman et al. (2003a)
H I Mass ($10^8 M_\odot$)	1.1 ± 0.1	Cannon et al. (2004)
$V_{H\text{el}io}$ (km s^{-1})	413 ± 5	Cannon et al. (2004)

^aGalactic longitude and latitude.

Table 2. Important Line Parameters

Line I.D.	λ_0^a (Å)	$\lambda_{\text{NGC 625}}$ (Å)	$\log(f \cdot \lambda)^a$	$V_{\text{NGC 625}}$ (km s ⁻¹)	$W_{\text{NGC 625}}^b$ (Å)	$\log(N)^c$
H ₂ L R(0)(2-0) ^d	1077.140	1078.60 ± 0.02	1.099	406 ± 6	0.07 ± 0.007	14.92 ± 0.19
H ₂ L R(1)(4-0) ^d	1049.960	1051.38 ± 0.03	1.213	406 ± 9	0.12 ± 0.01	15.01 ± 0.15
H ₂ L R(2)(5-0) ^d	1038.689	1040.07 ± 0.02	1.234	399 ± 6	0.04 ± 0.004	14.34 ± 0.19
H ₂ L P(1)(5-0) ^d	1038.157	1039.51 ± 0.02	0.954	391 ± 6	0.05 ± 0.005	14.82 ± 0.18
H ₂ W R(2)(0-0) ^d	1009.024	1010.36 ± 0.02	1.198	397 ± 6	0.05 ± 0.005	14.59 ± 0.18
H ₂ L R(1)(8-0) ^d	1002.449	1003.80 ± 0.03	1.262	404 ± 9	0.09 ± 0.009	14.87 ± 0.15
C II*	1037.018	1038.30 ± 0.02	2.088	371 ± 6	–	–
N I	1134.980	1136.43 ± 0.02	1.674	383 ± 6	0.10 ± 0.01	14.63 ± 0.12
N I	1134.415	1135.88 ± 0.02	1.512	387 ± 6	0.09 ± 0.009	< 14.80 ± 0.12
O I	1039.230	1040.55 ± 0.02	0.974	381 ± 6	0.24 ± 0.02	≥ 15.80 ± 0.12 ^e
O VI	1031.926	1033.20 ± 0.02	2.136	370 ± 6	0.20 ± 0.02	14.32 ± 0.08
Si II	1020.699	1022.03 ± 0.03	1.234	391 ± 9	0.19 ± 0.02	15.37 ± 0.15
P II	1152.818	1154.31 ± 0.02	2.451	388 ± 6	0.09 ± 0.009	13.54 ± 0.16
S III	1012.495	1013.79 ± 0.02	1.647	383 ± 6	0.38 ± 0.04	15.04 ± 0.15
Ar I	1066.660	1068.10 ± 0.02	1.857	405 ± 6	0.06 ± 0.006	14.20 ± 0.20
Ar I	1048.220	1049.58 ± 0.02	2.440	389 ± 6	0.12 ± 0.01	13.93 ± 0.10
Fe II	1144.938	1146.45 ± 0.02	1.978	396 ± 6	0.28 ± 0.03	14.72 ± 0.16
Fe II	1063.176	1064.61 ± 0.02	1.765	404 ± 6	0.17 ± 0.02	14.73 ± 0.15

^aAll atomic data are taken from Morton (2003). All molecular data is taken from the *H₂ools* website; see <http://www.pha.jhu.edu/~stephan/h2ools2.html> and McCandliss (2003).

^bRepresentative errors on the equivalent width values are ± 10%.

^cColumn densities derived from the apparent optical depth method; see Savage & Sembach (1991).

^dThe labels “L” and “W” denote Lyman or Werner bands, respectively.

^eThe O I λ 1039.230 Å line may be saturated; without a second oxygen line for comparison, there is no empirical way to test the saturation of this line. We note this uncertainty and discuss it further in § 3.3.3.

Table 3. Neutral vs. Nebular Abundances in Low-Metallicity Galaxies^a

Galaxy	Nebular [N/H] ^b	Neutral [N/H] ^c	Nebular [O/H] ^b	Neutral [O/H] ^c	Nebular log(N/O) ^b	Neutral log(N/O) ^c	$\Delta(\text{H I})$ (dex) ^d	Reference(s)
NGC 625	-1.07 ± 0.13	-1.80 ± 0.34	-0.47 ± 0.07	$\geq -1.36 \pm 0.33$	-1.33 ± 0.02	$\leq -1.17 \pm 0.15$	< -0.5	1, 2, 3
NGC 1705	-1.47 ± 0.14	-2.16 ± 0.24	-0.45 ± 0.07	-1.23 ± 0.22	-1.75 ± 0.06	-1.66 ± 0.11	-1.1	4, 5, 6
I Zw 18 ^e	-2.31 ± 0.13	-2.88 ± 0.11	-1.45 ± 0.05	-2.06 ± 0.28	-1.59 ± 0.05	-1.54 ± 0.26	$< +0.2$	7, 8, 9
I Zw 18 ^f	-2.31 ± 0.13	-3.00 ± 0.18	-1.45 ± 0.05	-1.36 ± 0.80	-1.59 ± 0.05	$-2.40^{+0.6}_{-0.8}$	$< +0.0$	7, 10, 9
I Zw 36	-1.65 ± 0.11	-2.81 ± 0.38	-0.89 ± 0.05	-1.76 ± 0.50^g	-1.49 ± 0.01	-1.80 ± 0.60^g	-0.2^h	11, 12, 13
Mrk 59	-1.46 ± 0.11	-2.08 ± 0.59	-0.67 ± 0.05	-1.66 ± 0.30	-1.52 ± 0.01	-1.15 ± 0.5	N/A ⁱ	11, 14

References. — 1 - Skillman et al. 2003b; 2 - This work; 3 - Cannon et al. 2004a; 4 - Lee & Skillman 2004; 5 - Heckman et al. 2001; 6 - Meurer et al. 1998; 7 - Skillman & Kennicutt 1993; 8 - Aloisi et al. 2003; 9 - van Zee et al. 1998; 10 - Lecavelier des Etangs et al. 2004; 11 - Izotov & Thuan 1999; 12 - Leboutteiller et al. 2004; 13 - Stil & Israel 2002; 14 - Thuan et al. 2002

^aThe abundances here use the solar nitrogen value from Holweger (2001) and the solar oxygen abundance from Asplund et al. (2004).

^bDerived from nebular spectroscopy of the most luminous H II regions in the galaxies, since these will be most heavily weighted in UV *FUSE* measurements.

^cDerived from *FUSE* spectroscopy.

^dDefined as the difference between the H I absorption column density toward the heavily-weighted UV sightlines as probed by *FUSE*, and the H I 21 cm emission column density (for the area nearest to the *FUSE* aperture): $\Delta(\text{H I}) = \log(N(\text{H I}))_{\text{FUSE}} - \log(N(\text{H I}))_{21 \text{ cm}}$.

^eNeutral gas values from analysis of *FUSE* data by Aloisi et al. (2003).

^fNeutral gas values from analysis of *FUSE* data by Lecavelier des Etangs et al. (2004).

^gCalculated using Phosphorus as a tracer of oxygen abundance; see discussion in Leboutteiller et al. (2004).

^hOnly peak H I 21 cm emission column density value is available; see Stil & Israel (2002).

ⁱDetailed H I emission observations of Mrk 59 are not yet available in the literature.